Electrochemical Behaviour of Graphene Oxide, Reduced Graphene Oxide and Zinc Oxide Graphene Oxide Composite Material Towards Fabrication of Dye Sensitized Solar Cell

SANDHYA MURALI[*] and A. JEYA RAJENDRAN

Advanced Materials Research Laboratory, Department of Chemistry, Loyola College (Affiliated to University of Madras), Chennai-600034, India

*Corresponding author: E-mail: sandhya_jn@hotmail.com

Graphene oxide (GO), reduced graphene oxide (rGO) and zinc oxide incorporated graphene oxide (ZnO-GO) nanoparticles were synthesized by wet-chemical technique. The ZnO-GO nanocomposite was synthesized from prepared graphene oxide. UV-visible and FTIR spectroscopy confirmed the presence of oxygen functionalities on graphene oxide which was reduced to rGO on treatment with the reducing agent. The XRD patterns revealed the formation of graphene oxide with a characteristic peak at 10.6° which shifted to 24° during the formation of rGO. The crystallite size of all the synthesized material was calculated using Scherrer's formula. The morphological behaviour of all materials was analyzed by scanning electron microscope (SEM). The electrochemical impedance data and Tafel plots suggested that the composite material has low charge transfer resistance (R_{ct}) and hence could act as a conducting material. The photoelectric conversion values, η for GO, rGO and ZnO-GO were calculated as 2.5, 5.7 and 7.5%, respectively and these values signify that the zinc oxide incorporated graphene oxide material has unique properties of electron transport.

Keywords: Graphene oxide, Reduced graphene oxide, Zinc oxide graphene oxide composite, Solar cell.

INTRODUCTION

Dye-sensitized solar cells (DSSCs) are a special kind of a low-cost photovoltaic cell that efficiently converts visible light into electrical energy. This type of cell mimics the photosynthesis process by absorbing natural light. In a dye sensitized solar cell, TiO_2 is used as conventional photoanode whereas platinum is the traditional counter electrode due to its high electrical conductivity, stability and desirable electro-chemistry, iodide/triiodide being the redox electrolyte. Research activities are focussed on finding alternative for fabricating Pt free counter electrode for DSSC. Different counter electrodes used in DSSCs include platinum based bulk, nanoparticles and composite materials, carbon material such as carbon black, amorphous carbon, mesoporous carbon, nanostuctured carbon (CNTs, graphene, nanofibres) [1-3].

Graphene is a novel material with great potential [4,5], which has a history that dates back to many decades where in the studies involved the chemistry of graphite [6-8]. The structure of graphite and its reactivity with potassium chlorate and fuming nitric acid were explored in 1859 [9]. The extent of oxidation was studied in detail and reported after 40 years [10]. Around 60 years later, Hummers and Offeman [11] developed an alternate oxidation method by reacting graphite with a mixture of $KMnO_4$ and conc. H_2SO_4. In Hummer's method, $KMnO_4$ is used as an oxidant but the active species is dimanganese heptoxide (Mn_2O_7). Graphene oxide (GO) is said to possess regular corrugated quinoidal structure interrupted by trans-linked cyclohexyl region, functionalised by tertiary alcohol and 1,3-ethers [12]. Graphene oxide (GO) is an electrically insulating material with disrupted sp^2 bonding networks. Electrical conductivity could be recovered by restoring the π-network , by the reduction of graphene oxide. Graphene oxide (GO) can be chemically reduced using hydrazine monohydrate [13]. Chemical reduction of GO restores the graphitic network in the basal plane of rGO. Graphene based material including graphene oxide metal oxide composites have been used as electrode material due to its high thermal and chemical stability, large surface area, excellent electrical conductivity and good thermal, mechanical properties. The large surface area enables it to be used in energy storage and energy conversion devices such as field effect transistors, solar cells, fuel cells, super capacitors, rechargeable

battery , optical modulators, chemical sensors, drug delivery and biomedical applications [14-25].

In this work, graphene oxide (GO), reduced graphene oxide (rGO) and ZnO incorporated graphene oxide (ZnO-GO) were prepared by wet chemical synthesis route followed by physical and electro-chemical characterization and used as photo-cathode in dye sensitized solar cell.

EXPERIMENTAL

All chemicals used were of analytical reagent grade and used without further purification. Graphite powder was procured from Loba, potassium permanganate, cetyl trimethylammonium bromide, zinc nitrate and sodium hydroxide were purchased from Merck. Concentrated sulphuric acid, phosphoric acid and hydrazine hydrate were procured from Merck. All the chemicals used were of 98% purity.

Fabrication of dye sensitized solar cell (DSSC): Graphene oxide was synthesized from graphite powder by modified Hummer's method [8] which was reduced by treatment with hydrazine hydrate. Graphene oxide was further used for the synthesis of ZnO incorporated GO composite material [26]. The photoanode was prepared using TiO_2 paste, which was coated on fluorine doped tin oxide (FTO) plates by Doctor blade technique [27]. The dried titanium dioxide film was soaked in 0.5mM N719 [di-tetrabutylammonium *cis-bis*(2,2'-bipyrodyl-4,4'-dicarboxylato)]ruthenium(II) dye. The counter electrode was prepared by using synthesized nanoparticles. Three different cathode were prepared using GO, rGO and ZnO GO. Solar cells were assembled by combining TiO_2 as active photoanode, GO, rGO and ZnO-GO as counter electrode and electrolyte, (I^-/I_3^-) was introduced between the two electrodes. The solar cells so prepared were then subjected to I-V studies using IVR electrometer.

Characterization: XRD patterns of the synthesized samples were recorded using XPERT PRO analytical instrument with a scan rate of 2 min^{-1}, an accelerating voltage of 40 kV, an applied current of 30 mA and using Cu$K\alpha$ radiation. The UV-visible spectra was analyzed using Jasco UV-Vis 2700 spectrophotometer. DRS measurements were carried out using a Cary 5000 UV-Vis-NIR spectrophotometer equipped with an integrated sphere. The Fourier transform infrared spectrum was analyzed using Shimadzu FTIR spectrophotometer. The morphologies of the samples were studied by a scanning electron microscope using TESCAN VEGA3 SBU VG825117IN. The electrochemical impedance spectroscopy (EIS) studies were carried out using LOGICS science instrument. Solar cells were fabricated and the current-voltage measurement of solar cells were studied by GS610 YOGOKAWA source measurement unit.

RESULTS AND DISCUSSION

UV-Visible analysis: UV-Visible analysis was used to confirm the reduction of graphene oxide. The spectrum of graphene oxide (Fig. 1) displayed a characteristic absorption band at 238 nm, which showed a red shift to 260 nm upon the formation of reduced graphene oxide.

UV-Vis diffuse reflectance spectroscopy was carried out to investigate the optical properties of the samples (Fig. 2).
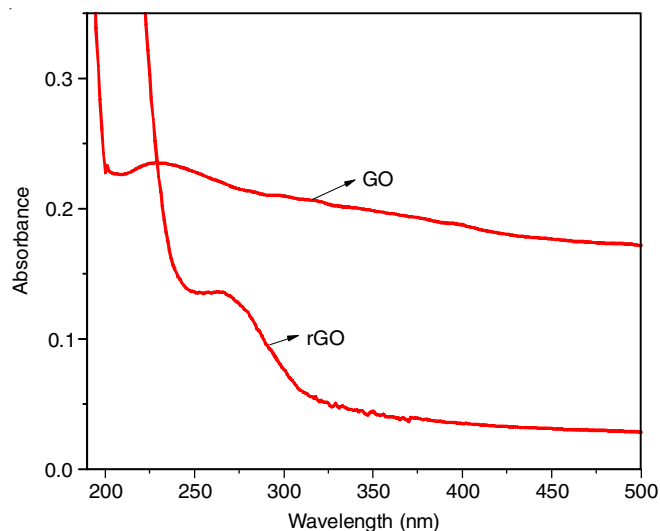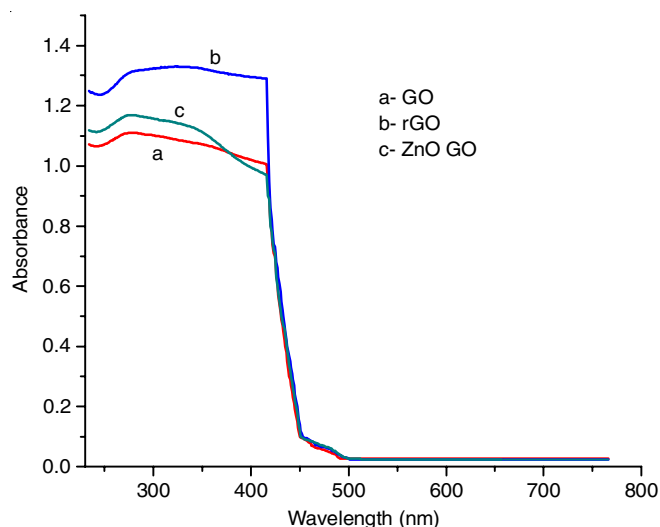

Fig. 1. UV-visible spectra of GO and rGO

Fig. 2. DRS spectra of GO, rGO and ZnO-GO

The band-gap energy was determined by using the relationship, $\alpha h\nu = A(h\nu - Eg)^n$, where h$\nu$ denotes photon energy, α the absorption coefficient, ($\alpha = 4\pi K/\lambda$) where, K denotes absorption index or absorbance, λ is the wavelength in nanometer), Eg is the energy band-gap and n is a constant equal to 1 for direct gap semiconductor and 4 for indirect gap semiconductor. The direct band gap energy was calculated using Tauc plot as 1.9 eV, 2.05 eV and 2.19 eV for GO, rGO and ZnO-GO, respectively.

FTIR analysis: The FTIR spectra of GO, rGO and ZnO-GO are shown in Fig. 3. The spectrum of GO displays peaks at 3412 cm^{-1} (broad peak due to O-H stretching in hydroxyl groups of GO), 1734 cm^{-1} (strong C=O stretching vibration), 1627 cm^{-1} (aromatic C=C bonds). Peaks at 1053 cm^{-1} corresponds to epoxy (C-O-C) and at 868 cm^{-1} may be due to C-O vibration of alkoxy group . The intensity of peaks were found to reduce in rGO due to the reduction of oxygen containing functional groups. The peaks at 3309 and 1764 cm^{-1} of composite material may be due to ν(OH) stretching of -C-OH and ν(-C=O) carbonyl stretching vibrations, respectively. The peak at 1699

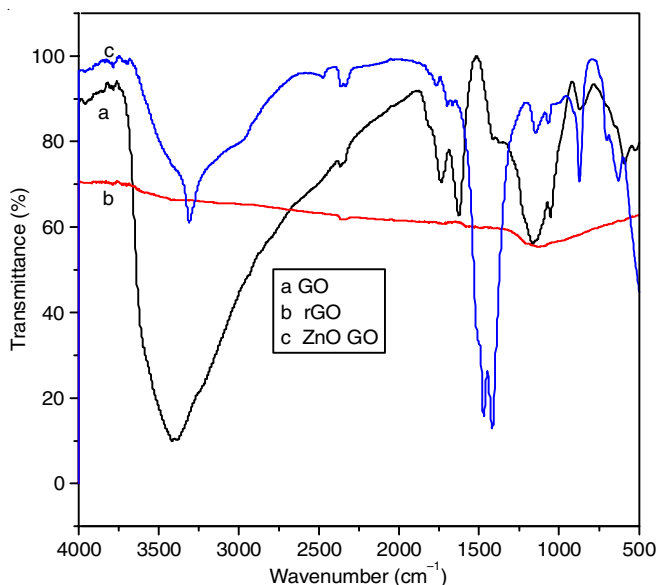Fig 3: FTIR spectra of (a) GO, (b) rGO and (c) ZnO doped GO

Fig. 4. XRD pattern of GO, rGO and ZnO doped GO

cm^{-1} corresponds to the aromatic C=C, peaks at 870 and 438 cm^{-1} may be due to Zn-O bonding and peaks at 629 cm^{-1} can be assigned to Zn-O-C bonding [28]. A peak at 702 cm^{-1} can be assigned to the C-O stretching vibration of alkoxy group and peak at 1068 cm^{-1} may be assigned to epoxy (C-O-C) stretching. The frequency shift observed may be attributed to the interaction of ZnO nanoparticles with GO. The absorption frequencies have been given in Table-1.

TABLE-1
ABSORPTION FREQUENCIES FROM FTIR SPECTRA

Functional groups	GO (cm^{-1})	rGO (cm^{-1})	ZnO-GO (cm^{-1})
O-H	3412	–	3309
C=O	1734	–	1764
Aromatic C=C	1627	–	1699
C-O-C	1053	1098	1068
C-O	868	–	702
Zn-O	–	–	438
Zn-O-C	–	–	629

XRD analysis: X-ray diffraction analysis was used to identify the phase, crystallinity and structure of synthesized material (GO, rGO, ZnO- GO) . The XRD pattern of GO (Fig. 4) exhibited a strong diffraction peak at 2θ value of 10.6º (002) plane with interlayer spacing of 0.83 nm (Fig. 4). This peak disappears in the XRD pattern of rGO which indicated that GO has been reduced to rGO. A relatively weak and broad peak of rGO (Fig. 4) is observed at 2θ = 24º , which is ascribed to the partial restacking of rGO sheets into an orderly crystalline structure. The characteristic diffraction peaks of zinc oxide incorporated graphene oxide is assigned to the hexagonal wurtzite structure with peaks at 23.0º, 31.7º, 34.4º, 37.16º, 47.36º, 57.04º, 62.52º and 69.1º corresponding to crystal planes of (100), (002), (101), (102), (110), (103), (201) and (200) (JCPDS no 36-1451) [29].

The crystallite grain size (D), dislocation density (δ) and strain (ε) were calculated for synthesized samples from XRD
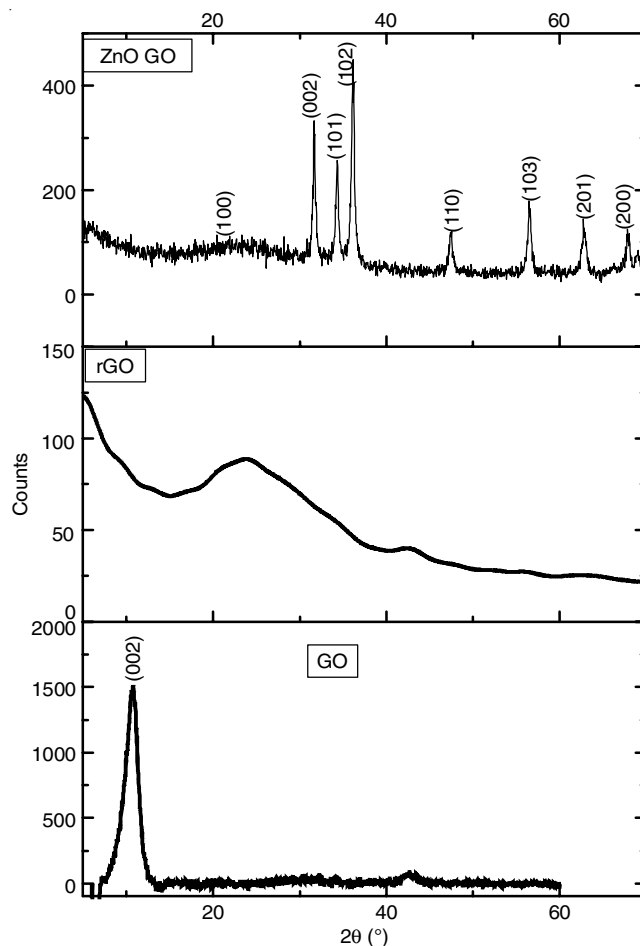
pattern. The crystallite grain size was calculated using Scherrer formula [30] (Table-2). The ZnO-GO material was found to have the least strain confirming more orderly and smooth surface, which could be used for coating FTO glass plates for light harvesting in solar cells.

TABLE-2
STRUCTURAL PARAMETERS FROM XRD

Materials	Crystallite size (nm)	Dislocation density (m^{-2})	Lattice strain (MPa)
GO	35.1	0.000812	0.00099
rGO	6.0	0.0278	0.005714
ZnO GO	42.9	0.000543	0.0008077

SEM analysis: The SEM images of GO, rGO , ZnO-GO revealed the morphology as layered structure (Figs 5a-b) for GO and curled and corrugated structure for reduced graphene oxide (Fig. 5c). The morphology of ZnO-GO material shows rod like structure along with porous base suggesting that zinc oxide nanoparticles have been impregnated in the layered structure of GO. The composition of the synthesized material was confirmed using EDAX analysis. Fig. 5d-e shows 96.6% carbon and 3.2% oxygen in the synthesized graphene oxide material.

EIS analysis: The resistance behaviour offered by GO, rGO and ZnO-GO electrode was investigated using electro-
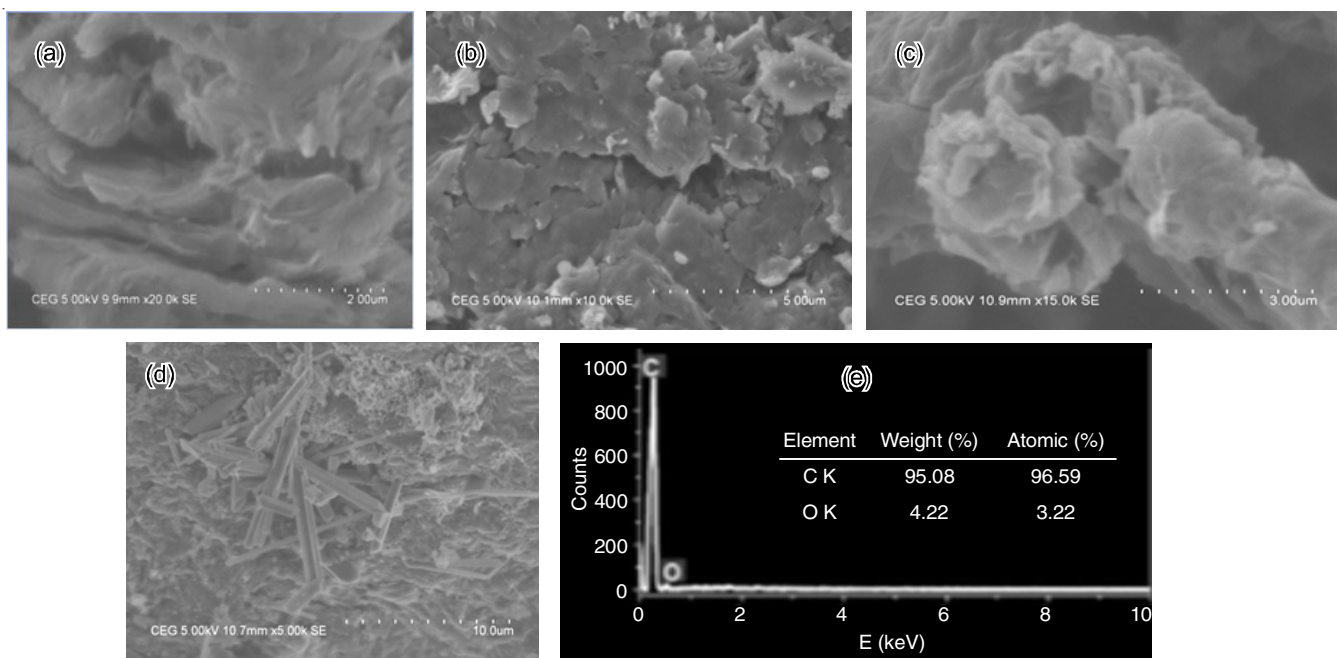
Fig. 5. SEM images of a), b) GO, c) rGO, d) ZnO doped GO e) EDX spectra of GO

chemical impedance spectroscopic (EIS) analysis within the frequency range 0-100 KHz at open circuit potential of 5 mV using 1M KOH. The Nyquist plot for all the material is illustrated in Fig. 6. The impedance plot exhibits semicircle at high frequency region. The diameter of the obtained semi-circle represent charge transfer resistance (R_{ct}). The diffusion process at the electrode- electrolyte interface is frequency dependent [31]. At high frequency region, the initial intersection point of the semicircle curve with the real impedance axis gives the solution resistance (R_s). It has been observed that graphene oxide shows R_s value of 0 Ω and R_{ct} value of 3900 Ω. The impedance spectrum of doped material is much smaller than the reduced graphene oxide indicating fast electron transfer process in the composite material. It also indicated that the composite material has lower resistance and better ion transport behaviour than both graphene oxide and reduced graphene

oxide. The EIS results showed that the composite material can enhance photovoltaic behaviour.

Tafel plots (Fig. 7) were used for evaluating kinetic parameters, which consists of an anodic and a cathodic branch. The anodic branch has a slope of $(1 - \alpha)F/23RT$ and the cathodic branch has a slope of $\alpha F/23RT$. The limiting current, J_o and diffusion co-efficient, D of the electrolyte were determined by using the following equations:

$$J_o = \frac{RT}{nFR_{ct}} \tag{1}$$

$$D = \frac{1}{2nF} \cdot J\,lim \tag{2}$$

where, T is the absolute temperature, n is the number of cycles, F is Faraday's constant, R_{ct} is the charge-transfer resistance,
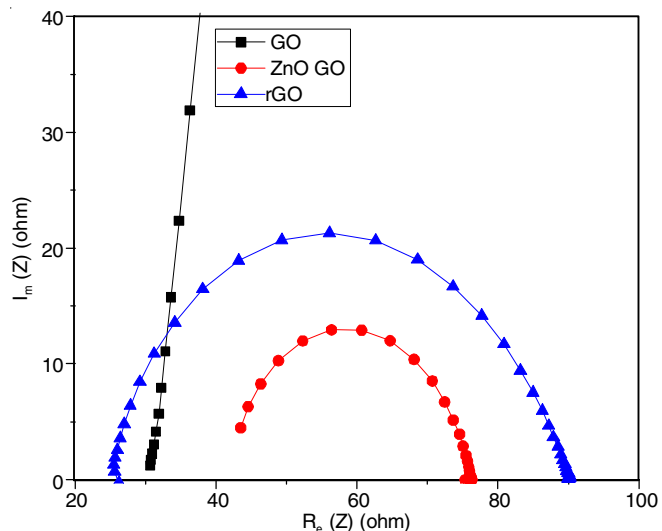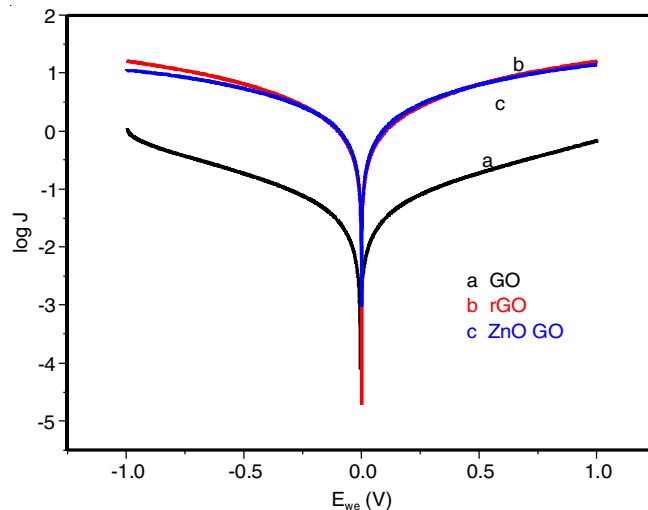

Fig. 6. EIS spectrum of GO, rGO and ZnO doped GO

Fig. 7. Tafel plot of GO, rGO and ZnO-GO

and l is the spacer thickness. Since J_o is inversely proportional to R_{ct}, the lower R_{ct} value at electrolyte-electrode surface, reduces the electron mass loss during charge transportation and enhances the photovoltaic parameters of dye sensitised solar cell (Table-3).

TABLE-3
TAFEL PARAMETERS OF GO, rGO, ZnO-GO

Material	log J_o	Cathodic slope	Anodic slope	α	R_{ct}
GO	0.137	1.3057	1.2559	0.0771	0.0581
rGO	0.3185	0.7866	0.8885	0.0442	0.0517
ZnO-GO	0.3613	0.7937	0.7376	0.0469	0.0297

Photovoltaic studies: The photovoltaic parameters, short circuit current (J_{sc}), open circuit voltage (V_{oc}), fill factor (FF) and power conversion efficiency (η) were calculated from the J-V plot of DSSC (Fig. 8), which was fabricated using TiO_2 as photoanode, GO, rGO and ZnO-GO as different photocathodes, I^-/I_3^- as electrolyte and ruthenium as dye are given in Table-4. The efficiency of a solar cell is defined as the output power density divided by the input power density. If the incoming light has a power density (P_{in}), the efficiency will be

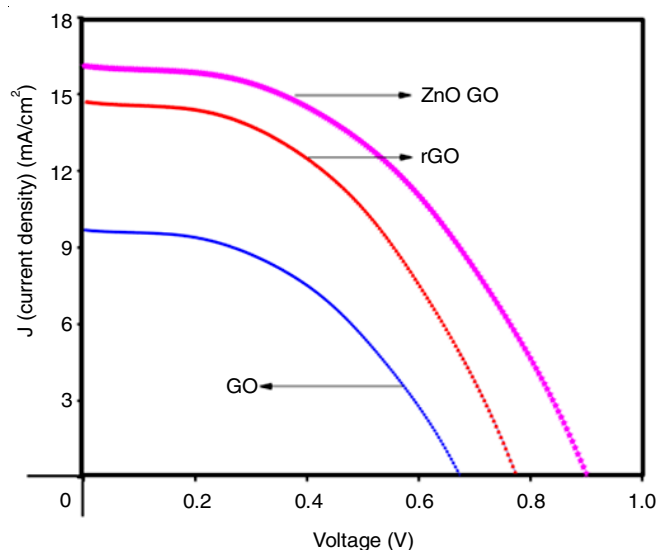$$\eta = \frac{V_{oc} \times J_{sc} \times FF}{Pin} \qquad (3)$$

Fig. 8.   J-V curve of the DSSC with TiO_2 as active electrode, GO, rGO and ZnO-GO as counter electrode

TABLE-4
PHOTOVOLTAIC PARAMETERS OF
THE GRAPHENE OXIDE BASED DSSC's

Parameters	GO	rGO	ZnO-GO
V_{oc} (V)	0.66	0.74	0.82
J_{sc} (mA)	9.8	14.7	16
FF	0.40	0.52	0.62
η (%)	2.5	5.7	7.5

The fill factor (FF) is defined as the ratio of the product of the maximum power output (P_m) to the product of short circuit photo current and open circuit

$$FF = \frac{I_{mp} \times J_{mp}}{V_{oc} \times J_{sc}} \qquad (4)$$

where I_{mp} and V_{mp} represent the photocurrent and photovoltage corresponding to the maximum power. The four parameters J_{sc}, V_{oc}, FF and η were used to characterize the performance of a solar cell which is given in Table-4.

Conclusion

Graphene oxide was synthesized from graphite using modified Hummer's method. The reduced graphene oxide (rGO) was prepared from synthesized graphene oxide (GO) by reducing with hydrazine hydrate and GO was converted to ZnO-GO using zinc nitrate. The synthesized materials were characterized using UV-Vis DRS spectroscopy. The band gap values suggested that the synthesized materials are good semiconductors. The structure was further confirmed using FTIR spectroscopy. The XRD analysis predicted the crystallite grain size. The morphology of samples were analyzed using SEM technique. The electrochemical behaviour was studied using impedance and Tafel plots. All the synthesized materials were used as photocathode to fabricate dye sensitized solar cells and photoconversion efficiency was measured as 2.5, 5.7 and 7.5% for GO, rGO and ZnO-GO, respectively. The electrochemical parameters suggested that metal oxide incorporated material could be used for photocurrent generation.

REFERENCES

1.   N. Mohanty and V. Berry, *Nano Lett.*, **8**, 4469 (2008);
      https://doi.org/10.1021/nl802412n
2.   Y. Yang, J. Wang, J. Zhang, J. Liu, X. Yang and H. Zhao, *Langmuir*, **25**, 11808 (2009);
      https://doi.org/10.1021/la901441p
3.   M. Fang, K. Wang, H. Lu, Y. Yang and S. Nutt, *J. Mater. Chem.*, **19**, 7098 (2009);
      https://doi.org/10.1039/b908220d
4.   A.K. Geim and K.S. Novoselov, *Nat. Mater.*, **6**, 183 (2007);
      https://doi.org/10.1038/nmat1849
5.   S. Park and R.S. Ruoff, *Nat. Nanotechnol.*, **4**, 217 (2009);
      https://doi.org/10.1038/nnano.2009.58
6.   V.C. Tung, M.J. Allen, Y. Yang and R.B. Kaner, *Nat. Nanotechnol.*, **4**, 25 (2009);
      https://doi.org/10.1038/nnano.2008.329
7.   H.P. Boehm and E. Stumpp, *Carbon*, **45**, 1381 (2007);
      https://doi.org/10.1016/j.carbon.2006.12.016
8.   C. Schafhaeutl, *J. Prakt. Chem.*, **21**, 129 (1840);
      https://doi.org/10.1002/prac.18400210117
9.   C. Schafhaeutl, *Lond. Edinb. Dublin Philos. Mag. J. Sci.*, **16**, 570 (1840);
      https://doi.org/10.1080/14786444008650094
10.   B.C. Brodie, *Philos. Trans. R. Soc. Lond.*, **149**, 249 (1859);
      https://doi.org/10.1098/rstl.1859.0013
11.   L. Staudenmaier, *Ber. Dtsch. Chem. Ges.*, **31**, 1481 (1898);
      https://doi.org/10.1002/cber.18980310237
12.   M. Dubois, J. Giraudet, K. Guérin, A. Hamwi, Z. Fawal, P. Pirotte and F. Masin, *J. Phys. Chem. B*, **110**, 11800 (2006);
      https://doi.org/10.1021/jp061291m
13.   W. Scholz and H.P. Boehm, *Z. Org. Allg. Chem.*, **369**, 327 (1969);
      https://doi.org/10.1002/zaac.19693690322

14. K.N. Kudin, B. Ozbas, H.C. Schniepp, R.K. Prud'homme, I.A. Aksay and R. Car, *Nano Lett.*, **8**, 36 (2008);
https://doi.org/10.1021/nl071822y

15. S. Park, D.A. Dikin, S.T. Nguyen and R.S. Ruoff, *J. Phys. Chem. C*, **113**, 15801 (2009);
https://doi.org/10.1021/jp907613s

16. S. Park, K.S. Lee, G. Bozoklu, W. Cai, S.T. Nguyen and R.S. Ruoff, *ACS Nano*, **2**, 572 (2008);
https://doi.org/10.1021/nn700349a

17. J.T. Robinson, M. Zalalutdinov, J.W. Baldwin, E.S. Snow, Z. Wei, P. Sheehan and B.H. Houston, *Nano Lett.*, **8**, 3441 (2008);
https://doi.org/10.1021/nl8023092

18. R.S. Sundaram, C. GómezNavarro, K. Balasubramanian, M. Burghard and K. Kern, *Adv. Mater.*, **20**, 3050 (2008);
https://doi.org/10.1002/adma.200800198

19. M. Zhou, Y. Wang, Y. Zhai, J. Zhai, W. Ren, F. Wang and S. Dong, *Chem. Eur. J.*, **15**, 6116 (2009);
https://doi.org/10.1002/chem.200900596

20. S. Niyogi, E. Bekyarova, M.E. Itkis, J.L. McWilliams, M. Hamon and R.C. Haddon, *J. Am. Chem. Soc.*, **128**, 7720 (2006);
https://doi.org/10.1021/ja060680r

21. Y. Xu, Z. Liu, X. Zhang, Y. Wang, J. Tian, Y. Huang, Y. Ma, X. Zhang and Y. Chen, *Adv. Mater.*, **21**, 1275 (2009);
https://doi.org/10.1002/adma.200801617

22. Z.B. Liu, Y.F. Xu, X.Y. Zhang, X.L. Zhang, Y.S. Chen and J.G. Tian, *J. Phys. Chem. B*, **113**, 9681 (2009);
https://doi.org/10.1021/jp9004357

23. X. Zhang, Y. Huang, Y. Wang, Y. Ma, Z. Liu and Y. Chen, *Carbon*, **47**, 334 (2009);
https://doi.org/10.1016/j.carbon.2008.10.018

24. Z. Liu, J.T. Robinson, X. Sun and H. Dai, *J. Am. Chem. Soc.*, **130**, 10876 (2008);
https://doi.org/10.1021/ja803688x

25. L.M. Veca, F. Lu, M.J. Meziani, L. Cao, P. Zhang, G. Qi, L. Qu, M. Shrestha and Y.-P. Sun, *Chem. Commun.*, **18**, 2565 (2009);
https://doi.org/10.1039/b900590k

26. X. Zhou, T. Shi and H. Zhou, *Appl. Surf. Sci.*, **258**, 6204 (2012);
https://doi.org/10.1016/j.apsusc.2012.02.131

27. K.P. Bhandari, P.J. Roland, H. Mahabaduge, N.O. Haugen, C.R. Grice, S. Jeong, T. Dykstra, J. Gao and R.J. Ellingson, *Sol. Energy Mater. Sol. Cells*, **117**, 476 (2013);
https://doi.org/10.1016/j.solmat.2013.07.018

28. Y. Yang and T. Liu, *Appl. Surf. Sci.*, **257**, 8950 (2011);
https://doi.org/10.1016/j.apsusc.2011.05.070

29. J. Zhang, L. Sun, C. Liao and C. Yan, *Chem. Commun.*, **3**, 262 (2002);
https://doi.org/10.1039/b108863g

30. S. Tiwari and S. Tiwari, *Sol. Energy Mater. Sol. Cells*, **90**, 1621 (2006);
https://doi.org/10.1016/j.solmat.2005.01.021

31. Z. Fan, K. Wang, T. Wei, J. Yan, L. Song and B. Shao, *Carbon*, **48**, 1686 (2010);
https://doi.org/10.1016/j.carbon.2009.12.063